






## Article

# Protective Effect of Oyaksoongi-San against Asthma Induced by Ovalbumin in a Mouse Model

Jun-Yeop Song <sup>1</sup>, Eun-Bok Baek <sup>1</sup>, Eun-Ju Hong <sup>1</sup>, Poornima Kumbukghadeniya <sup>1</sup>, Yu-Jin Kim <sup>2</sup>, Mee-Young Lee <sup>2</sup> and Hyo-Jung Kwun <sup>1,\*</sup>

<sup>1</sup> Department of Veterinary Pathology, College of Veterinary Medicine, Chungnam National University, Daejeon 34134, Republic of Korea; qldqld0610@gmail.com (J.-Y.S.)

<sup>2</sup> KM Convergence Research Division, Korea Institute of Oriental Medicine, Daejeon 34054, Republic of Korea

\* Correspondence: hyojung@cnu.ac.kr; Tel.: +82-42-821-7403; Fax: +82-42-821-8903

**Abstract:** Oyaksoongi-San (OYSGS), which is a combination of 11 herbal ingredients, has long been used in Asia to relieve symptoms of various diseases conditions, including vomiting and diarrhea. In this study, we assessed the protective efficacy of OYSGS in a murine model of asthma induced by ovalbumin (OVA) and explored potential molecular mechanisms. Male C57BL/6 mice were sensitized with OVA and airway challenged with OVA (1% *w/v* in PBS) for 1 h. OYSGS (100, 300, and 500 mg/kg once daily) was administered for 6 days by oral gavage. Our results revealed that OYSGS significantly decreased the number of inflammatory cells and reduced the concentrations of interleukin (IL)-5 and IL-13 in bronchoalveolar lavage fluid (BALF). Histological analyses showed that OYSGS substantially decreased inflammation and mucus hypersecretion in the airway. Further analyses revealed that OYSGS effectively reduced oxidative stress, as shown by downregulation of malondialdehyde (MDA) and upregulation of total glutathione (GSSG/GSH), and markedly suppressed the phosphorylation of p38 mitogen-activated protein kinase (p38 MAPK). Together, these results suggest that OYSGS effectively inhibits the airway inflammatory responses, mucus secretion, and oxidative stress induced by OVA.

**Keywords:** asthma; Oyaksoongi-San; ovalbumin; inflammation; mucus secretion; oxidative stress; p38 MAPK



**Citation:** Song, J.-Y.; Baek, E.-B.; Hong, E.-J.; Kumbukghadeniya, P.; Kim, Y.-J.; Lee, M.-Y.; Kwun, H.-J. Protective Effect of Oyaksoongi-San against Asthma Induced by Ovalbumin in a Mouse Model. *Appl. Sci.* **2024**, *14*, 5280. <https://doi.org/10.3390/app14125280>

Academic Editors: Jose Antonio Cañas and Blanca Cárdbaba

Received: 24 May 2024  
Revised: 11 June 2024  
Accepted: 16 June 2024  
Published: 18 June 2024



**Copyright:** © 2024 by the authors. Licensee MDPI, Basel, Switzerland. This article is an open access article distributed under the terms and conditions of the Creative Commons Attribution (CC BY) license (<https://creativecommons.org/licenses/by/4.0/>).

## 1. Introduction

Asthma is a prevalent chronic respiratory condition that impacts millions worldwide and remains a subject of ongoing research and medical treatments. It manifests as airway hypersensitivity to various triggers, leading to symptoms such as breathlessness, wheezing, coughing, and chest tightness [1], and varies across individuals. However, asthma has common underlying mechanisms, making it a captivating subject for scientific investigation. The triggers of asthma include environmental and genetic factors. Common environmental triggers are allergens like pollen, dust mites, and pet dander [1]. Researchers must thoroughly understand the disease as they seek to develop innovative treatment approaches that target both symptom relief and the underlying origins. Pathophysiologically, asthma is an inflammatory disease in which T-helper type 2 (Th2) cell-secreted cytokines induce the proliferation of inflammatory cells which migrate to and infiltrate the airways [2]. These inflammatory cells trigger excessive mucus production, causing further airway constriction and posing significant challenges to effective airflow [3]. The accumulation of excessive mucus both obstructs the airways and creates an environment conducive to exacerbations. Thus, it is important to address mucus-related complications as an integral component of comprehensive asthma management strategies [4]. Oxidative stress, which is also closely related to asthma, occurs when the production of reactive oxygen species (ROS) surpasses the body's antioxidant capacity, leading to cellular damage and dysregulation of redox

signaling pathways. This imbalance is implicated in various pathological conditions that are central to asthma [5]. Oxidative stress also contributes to the chronicity of asthma [6].

Extensive research is underway on the various dosages of corticosteroids to alleviate asthma symptoms and target its underlying causes, yet comprehensive solutions remain elusive [7]. Minimizing exposure to triggers, such as allergens and respiratory irritants, can help manage asthma symptoms. If inhaled corticosteroids are insufficient and symptoms persist, long-acting beta agonists (LABAs) or anti-leukotriene agents may be added [8]. However, despite the development of various therapies, the rising prevalence of asthma and its associated mortality continue to underscore the need for a treatment that fundamentally targets the asthma pathogenesis [9].

The herbal formulation Oyaksoongi-San (OYSGS) is a traditional substance employed to prevent and treat a wide array of illnesses. For example, patients with cerebral infarction showed substantial reductions in the secretions of pro- and anti-inflammatory factors by peripheral blood mononuclear cells following pretreatment with OYSGS [10]. Other studies have shown that OYSGS inhibits colon cancer cell proliferation [11] and alleviates refractory chronic pain in trigeminal neuralgia, as shown in a single patient [12]. OYSGS is composed of 11 extracts: Angelica dahurica root, Aurantii fructus immaturus, Batryticatus bombyx, Citrus unshiu peel, Cnidium rhizome, Ephedra herb, ginger, jujube, licorice, Lindera root, and Platycodon root. These constituent herbal ingredients have been shown to exhibit a range of pharmacological properties [13–20].

Nevertheless, there has been no prior investigation into the potential of OYSGS for enhancing or managing asthma. Here, we examined the possible therapeutic effects of OYSGS in a murine model of ovalbumin-induced asthma and explored potential underlying mechanisms.

## 2. Materials and Methods

### 2.1. Chemicals and Reagents

Commercially available OYSGS granules were obtained from Korea Syntex Pharmaceutical (Iksan, Republic of Korea). All reference standards (purities > 95%) used to identify and quantify the phytochemicals in OYSGS were purchased from ChemFaces Biochemical Co., Ltd. (Wuhan, China), with the exception of ephedrine (Sigma-Aldrich, St. Louis, MO, USA). The MS-grade water, acetonitrile, methanol, and formic acid were purchased from Thermo Fisher Scientific (Waltham, MA, USA).

### 2.2. Preparation of Sample and Standard Solutions

OYSGS was dissolved in methanol at 0.05, 0.1, 0.5, and 20 mg/mL and filtered through a syringe filter (0.2 µm pore size). All reference standards were serially diluted with methanol to final concentrations of 0.02–10 µg/mL for UPLC-DAD-MS/MS analysis.

### 2.3. Ultra-Performance Liquid Chromatography–Diode Array Detector–Tandem Mass Spectrometry (UPLC-DAD-MS/MS) Conditions

To identify and quantify the compounds in OYSGS, a Dionex UltiMate 3000 system equipped with a Thermo Q-Exactive mass spectrometer was used. The UPLC-DAD-MS/MS analysis was performed with slight modifications from the previously reported methods [21,22]. The compounds were separated on an Acquity BEH C<sub>18</sub> column (150 × 2.1 mm, 1.7 µm, Waters) at 40 °C. The mobile phase consisting of solvents A (0.1% (v/v) aqueous formic acid) and B (acetonitrile) was eluted with the following gradient at a flow rate of 0.25 mL/min: 3% B for 0–1 min, 3–15% B for 1–2 min, 15–25% B for 2–10 min, 25–45% B for 10–15 min, 45–100% B for 15–20 min, 100% B for 20–23 min, and 3% B for 24–28 min. The injection volume was 3 µL. The Q-Exactive mass spectrometer equipped with an electrospray ionization (ESI) source was operated in both positive and negative ionization modes with an ion spray voltage of 3.8 kV, capillary temperature of 320 °C, sheath gas pressure of 40 arbitrary units (au), auxiliary gas pressure of 10 au, and S-lens RF level of 60. The resolutions of the MS1 and MS/MS scans were 70,000 and 17,500, respectively. Mass spectra

were recorded in the range of 100–1500  $m/z$ , and the collision energies of each analyte are shown in Table S1. Data-dependent acquisition using the full MS-ddMS<sup>2</sup> setup was used. Xcalibur v.3.0 and Tracefinder v.3.2 software were used to process the acquired data.

#### 2.4. Animals

Six-week-old male C57BL/6 mice were obtained from a laboratory animal supplier and acclimated for 1 week with ad libitum access to solid food and water under conditions of  $20 \pm 2$  °C,  $50 \pm 10\%$  relative humidity, and a 12 h light and dark cycle. Animal experiments were conducted in compliance with the guidelines set forth by the Institutional Animal Care and Use Committee of Chungnam National University.

#### 2.5. Induction of Asthma

Ovalbumin (OVA, 20 µg) was dissolved in 200 µL of phosphate-buffered saline (PBS) and mixed with 2 mg aluminum hydroxide (Alum), and 200 µL of the generated OVA/Alum was administered intraperitoneally to mice on days 0 and 14 for systemic sensitization. Local sensitization was performed on days 21 and 23 by causing mice to inhale 1% OVA for 1 h using a nebulizer (NE-U12; Omron Corp., Tokyo, Japan) to create the asthmatic mouse model. Animals were randomly allocated to the following ( $n = 7$  per group): (i) negative control group treated with PBS (NC), (ii) OVA administration group (OVA), (iii) OVA administration and dexamethasone (DEX) treatment (1 µg/100 mL per mouse) group as a positive control (OVA+DEX), and (iv, v, vi) OVA administration and OYSGS treatment (100, 300, and 500 mg/kg, respectively) groups (OVA+OYSGS100, 300, and 500, respectively). DEX (200 µg, Sigma-Aldrich, St. Louis, MO, USA) and OYSGS were dissolved in PBS 20 mL and administered daily by oral gavage at 0.125 mL per animal using a 1 mL syringe with a metal zonde, from days 18 to 23 of the experiment. All mice were sacrificed on day 25.

#### 2.6. Necropsy and Histopathological Examination

Lung tissues were fixed in 10% buffered neutral formalin, sliced, paraffin embedded, and sectioned at 4 µm using conventional tissue-processing methods. The sections were hematoxylin and eosin (H&E) stained. The tissues were examined for inflammatory cell infiltration and inflammation scoring [23], which was performed as previously described [24]. In summary, the severity of inflammation was assessed using a 0–5 scale. A score of 0 represented normal tissue with no inflammation. A score of 1 indicated mild inflammation with small clusters of inflammatory cells. A score of 2 corresponded to mild ring-shaped infiltration of inflammatory cells, forming a layer one cell in thickness. A score of 3 was given for moderate ring-shaped infiltration with a layer two to four cells in thickness. A score of 4 represented severe ring-shaped infiltration with a layer four cells in thickness. Finally, a score of 5 indicated very severe inflammation with extensive infiltration and a loss of the normal tissue structure. Tissue sections were also exposed to periodic acid–Schiff (PAS) staining, images were randomly selected, and the positive area (%) was analyzed relative to the total area of bronchial epithelium.

#### 2.7. Microscopic Analysis of Inflammation-Associated Cells in Bronchoalveolar Lavage Fluid (BALF)

BALF was obtained by three rounds of aspiration (0.5 mL per round) using a tracheally inserted cannula, and 100 µL was placed on a slide. The cells were fixed by centrifugation in a cytospin and stained with trypan blue, and the total number of cells, excluding dead cells, was calculated using a hemocytometer and measured in triplicate. Inflammatory cell staining was conducted using Diff Quik reagents (IMEB, San Marcos, CA, USA), followed by differentiation of individual cells based on their morphology to determine the numbers of neutrophils, lymphocytes, macrophages, and eosinophils.

### 2.8. Enzyme-Linked Immunosorbent Assay (ELISA)

IL-5 and IL-13 levels in BALF and malondialdehyde (MDA) and total glutathione (GSSG/GSH) levels in lung tissues were quantified using commercially available ELISA kits (IL-5, IL-13: R&D Systems, Minneapolis, MN, USA; MDA, total glutathione: Cell Biolabs, CA, USA) according to the manufacturers' instructions [25–30]. To summarize, the samples were lysed and centrifuged, after which 50  $\mu$ L of the supernatants was promptly dispensed into the wells of assay plates and incubated at room temperature for 2 h. The plates were then washed using the wash solution provided in the kit. Following this, conjugates were added to each well and allowed to incubate for another 2 h. Relative cytokine levels were quantified by performing duplicate measurements. The plates were incubated in the dark for 10 min, and absorbance was quantified using a microplate reader (Infinite m200pro; TECAN, Männedorf, Switzerland).

### 2.9. RNA Extraction and Real-Time PCR Analysis

Real-time PCR was utilized to determine the levels of MUC5AC expression in the lungs [31]. Lung tissues were homogenized, and RNA extraction was carried out using TRIzol (Invitrogen, Richardson, TX, USA). The RNA concentration was assessed through absorbance measurement at 260 nm, while its purity was evaluated using the 260 nm/280 nm ratio. cDNA was synthesized through the use of a commercial kit (Toyobo, Osaka, Japan). PCR amplification was conducted using a Real-Time PCR machine (Life Technologies, Frederick, MD, USA), SYBR Green (Applied Biosystems, Richardson, TX, USA), and MUC5AC primers, 5'-CCA CTT TCT CCT TCT CCA CAC C-3' (forward) and 5'-GGT TGT CGA TGC AGC CTT GCT T-3' (reverse). The data were analyzed utilizing Applied Biosystems PCR System software (v1.5.3). The fold change in target gene cDNA expression relative to the endogenous control (GAPDH) was determined using the  $2^{-\Delta\Delta C_t}$  method.

### 2.10. Western Blot Analysis

Lysis of lung tissues was carried out with RIPA lysis buffer (Cell Signaling Technology, Danvers, MA, USA) containing inhibitor cocktails. Equal amounts of lung proteins (30  $\mu$ g) were resolved by 8% SDS-PAGE at 60V and transferred to a polyvinylidene fluoride (PVDF) membrane at 250V for 2 h. Transferred membranes were treated with PBS containing 0.05% Tween 20 (PBST) and 5% skim milk for 1 h for blocking, incubated overnight at 4 °C with anti-p38 MAPK and anti-phospho-p38 MAPK (Cell Signaling Technology, Danvers, MA, USA), or anti- $\beta$ -actin (Sigma-Aldrich, St. Louis, MO, USA), and incubated with secondary antibodies for 2 h at room temperature. The results were visualized using a luminograph (ATTO, Tokyo, Japan).

### 2.11. Immunohistochemistry (IHC) Assay

MUC5AC expression in lung tissue was assessed by IHC [32], which was performed as previously described [33]. Anti-MUC5AC (Sigma-Aldrich, St. Louis, MO, USA) was applied overnight, and signals were developed and visualized based on the established protocol. The signal-positive area was quantitatively analyzed using Image J software (v 1.53k).

### 2.12. Statistical Analysis

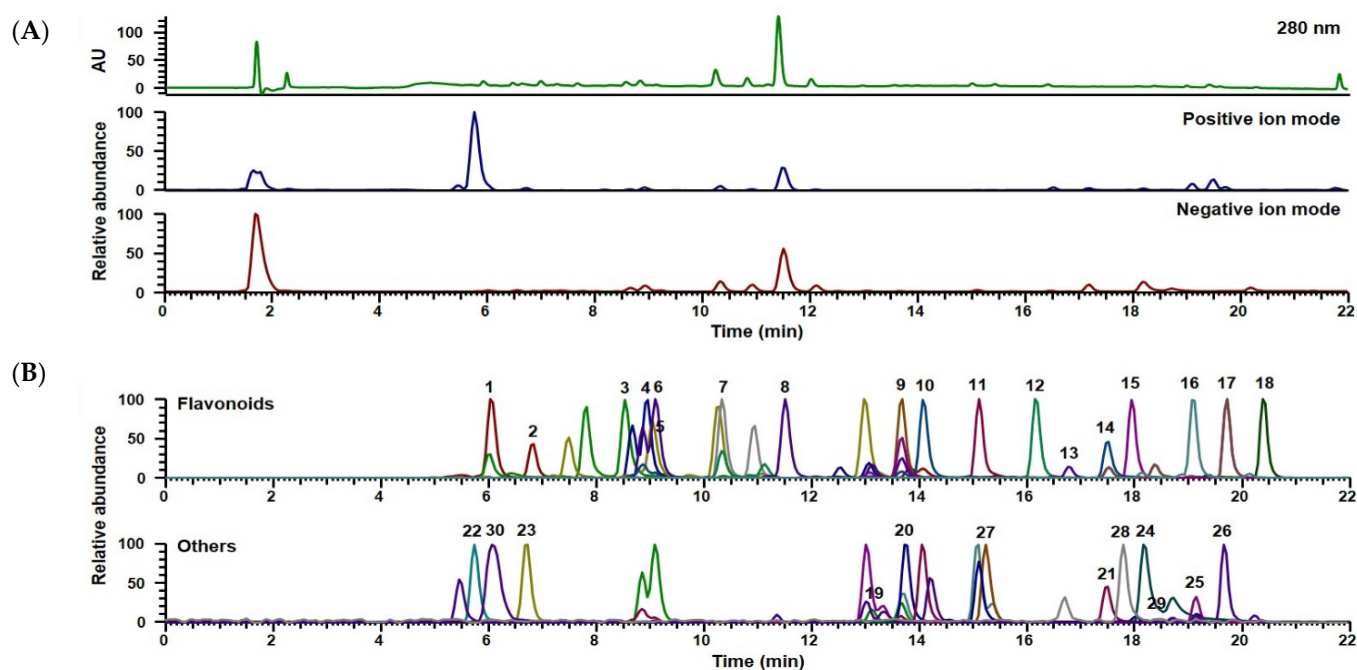
The data are expressed as mean  $\pm$  standard deviation (SD). Statistical analysis was conducted using one-way analysis of variance (ANOVA), as applied by the GraphPad Prism 6 software (GraphPad, San Diego, CA, USA), followed by Tukey's multiple-comparison test. A *p*-value < 0.05 was regarded as statistically significant.

## 3. Results

### 3.1. UPLC-DAD-MS/MS Analysis of OYSGS

Previous phytochemical studies showed that OYSGS contains various types of secondary metabolites, such as flavonoids, alkaloids, terpenoids, coumarins, and other phenolic compounds [22,34–42]. By comparing with reference standards' retention times and

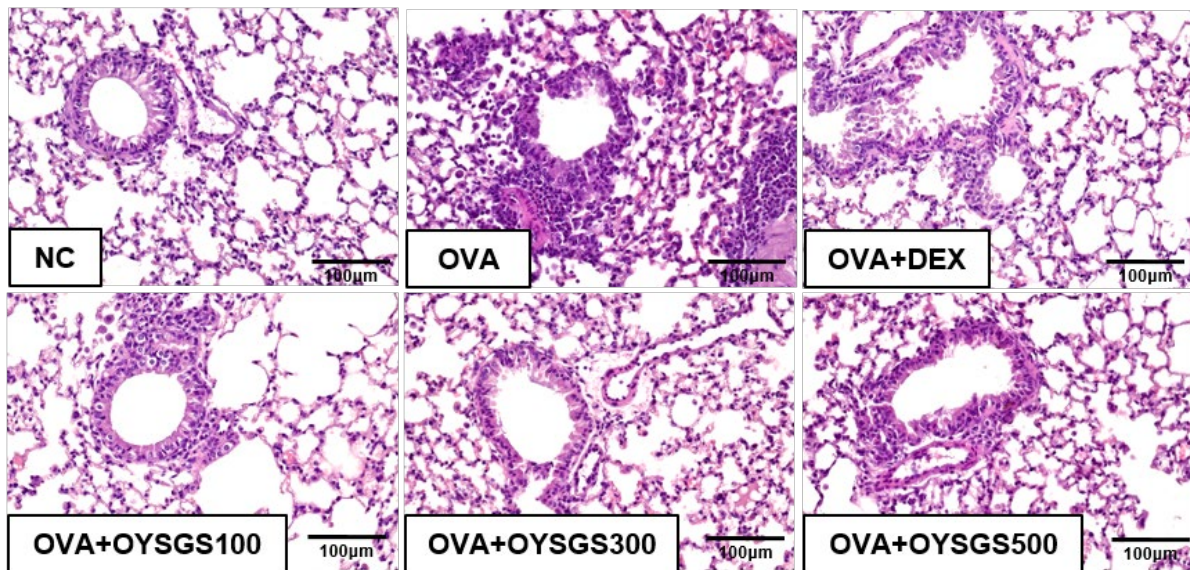
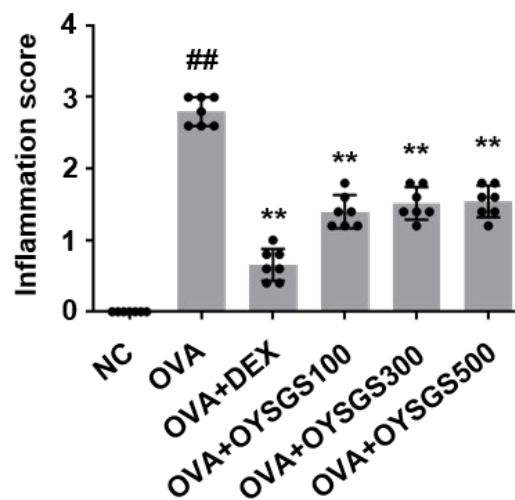
mass spectra, thirty phytochemical constituents were identified. They were as follows: 18 flavonoids (catechin, epicatechin, rutin, and isoquercitrin/hyperoside from *Zizyphi Fructus* [34,35], liquiritin apioside, liquiritin, ononin, liquiritigenin, naringenin, formononetin, and glabridin from *Glycyrrhizae Radix* [36], narirutin, hesperidin, didymin, hesperetin, nobiletin, and tangeretin from *Citri Unshius Pericarpium* [37,38], and isosinensetin from *Aurantii Fructus Immaturus* [39]), three chalcones (isoliquiritin, licochalcone B, and isoliquiritigenin from *Glycyrrhizae Radix* [36]), two alkaloids (ephedrine from *Ephedrae Herba* [40] and norisoboldine from *Linderae Radix* [41]), three terpenoids (glycyrrhizin from *Glycyrrhizae Radix* [36], nomilin and obacunone from *Aurantii Fructus Immaturus* [22]), three coumarins (byakangelicin, bergapten, and pabulenol from *Angelicae Dahuricae Radix* [42]), and one phenylpropanoid (chlorogenic acid from *Citri Unshius Pericarpium* [37]). Figure 1A presents the UV spectra at 280 nm and the base peak ion chromatograms of OYSGS in positive and negative ion modes, while extracted ion chromatograms for individual compounds are depicted in Figure 1B. The characteristics of the compounds identified in OYSGS, including the retention time ( $t_R$ ), precursor ion ( $m/z$ ), error (ppm), molecular formula, MS/MS fragments, and contents of each, are summarized in Table S1. Flavonoids, chalcones, and phenylpropanoid were better detected in the negative ion mode, while alkaloids, terpenoids, and coumarins were better detected in the positive ion mode. Twenty-three of the phytochemicals were present in amounts ranging from 0.001 to 1.421 mg/g; the outliers were isoquercitrin (or hyperoside), formononetin, isoliquiritigenin, glycyrrhizin, bergapten, pabulenol, and chlorogenic acid.



**Figure 1.** UPLC-DAD-MS/MS analysis of OYSGS. (A) UV (280 nm) and base peak ion chromatograms (positive and negative ion modes) of OYSGS and (B) extracted ion chromatogram (XIC) of the phytochemicals identified in OYSGS. The numbered compounds are named and presented in detail in Table S1.

### 3.2. Histopathologic Analysis of Lung Tissues

H&E staining revealed more inflammatory cells around the bronchi and bronchioles in the OVA group compared to the NC group, but this enhancement of inflammatory cell infiltration was reduced in tissues from the OVA+DEX and OVA+OYSGS groups (Figure 2A,B). The changes did not appear to track with the concentration of OYSGS. These results show that OYSGS effectively attenuates OVA-induced inflammation.

**A****B**

**Figure 2.** Effect of OYSGS on the recruitment of inflammatory cells to the airway. (A) Lung tissues with H&E staining. Scale bar, 100  $\mu$ m; magnification, 200 $\times$  (B) Inflammation scored from 0 (absent) to 4 (severe). NC, negative control; OVA, ovalbumin-exposed mice; OVA+DEX, dexamethasone-administered and OVA-exposed mice; OVA+OYSGS100, OYSGS- (100 mg/kg) and OVA-exposed mice; OVA+OYSGS300, OYSGS- (300 mg/kg) and OVA-exposed mice; OVA+OYSGS500, OYSGS- (500 mg/kg) and OVA-exposed mice. Results are presented as means  $\pm$  SD (##  $p < 0.01$  compared with the NC group; \*\*  $p < 0.01$  compared with the OVA group).

### 3.3. Analysis of Inflammatory Cells in BALF

The numbers of total cells, macrophages, lymphocytes, neutrophils, and eosinophils were markedly increased in BALF of the OVA group compared to the NC group. These enhancements were significantly reduced in the OVA+DEX and OVA+OYSGS groups (Figure 3), without evidence of dose dependence for OYSGS.

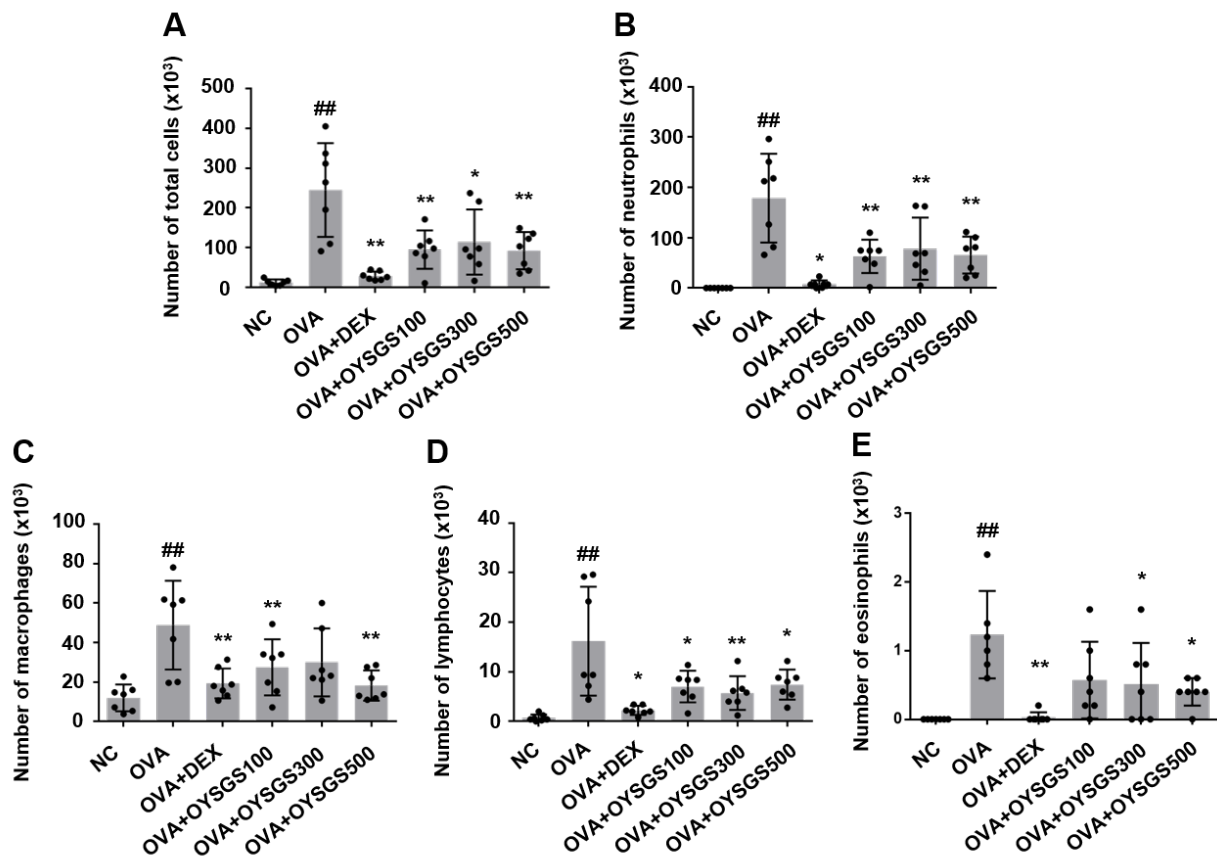


**Figure 3.** Effect of OYSGS on inflammatory cell counts in BALF. (A–D) Numbers of (A) total cells, (B) neutrophils, (C) macrophages, (D) lymphocytes, and (E) eosinophils. NC, negative control; OVA, ovalbumin-exposed mice; OVA+DEX, dexamethasone-administered and OVA-exposed mice; OVA+OYSGS100, OYSGS- (100 mg/kg) and OVA-exposed mice; OVA+OYSGS300, OYSGS- (300 mg/kg) and OVA-exposed mice; OVA+OYSGS500, OYSGS- (500 mg/kg) and OVA-exposed mice. Results are presented as means  $\pm$  SD (##  $p < 0.01$  compared with the NC group; \*  $p < 0.05$ , \*\*  $p < 0.01$  compared with the OVA group).

### 3.4. Analysis of Cytokine Production in BALF

Th2 cytokines in BALF were quantified using ELISA. The levels of IL-5 and IL-13 in BALF were increased in the OVA group compared to the NC group, and these enhancements were notably reduced in the OVA+DEX and OVA+OYSGS groups (Figure 4A,B), without evidence of dose dependence for OYSGS.

### 3.5. Analysis of Mucus Production in Lung Tissues

PAS staining of glycoproteins in bronchiolar epithelial cells revealed that the PAS-positive area was increased in the OVA group when compared with the NC group, and this enhancement was substantially decreased in the OVA+DEX and OVA+OYSGS groups (Figure 5A,C). In IHC, the MUC5AC-positive area was increased in the OVA group compared with the NC group, and this enhancement was markedly decreased in the OVA+DEX and OVA+OYSGS groups (Figure 5B,D). Consistently, the relative mRNA expression of MUC5AC in lung tissues was also increased in the OVA group compared to the NC group, and it was significantly decreased in the OVA+DEX and OVA+OYSGS groups compared to the OVA group (Figure 5E). The effects of OYSGS did not show evidence of dose dependence. Thus, our results indicated that OYSGS significantly attenuates OVA-induced mucus secretion in mice.

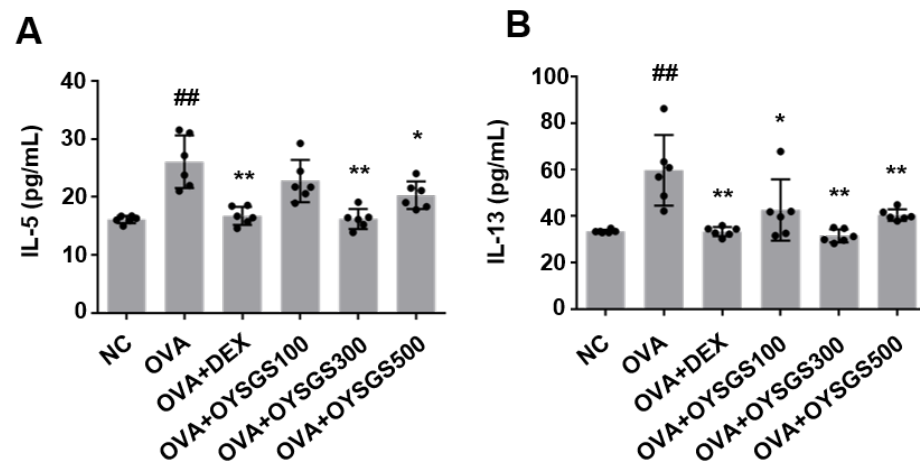


**Figure 4.** Effect of OYSGS on pro-inflammatory cytokine levels in BALF. (A,B) IL-5 (A) and IL-13 (B) levels, as assessed using ELISA. NC, negative control; OVA, ovalbumin-exposed mice; OVA+DEX, dexamethasone-administered and OVA-exposed mice; OVA+OYSGS100, OYSGS- (100 mg/kg) and OVA-exposed mice; OVA+OYSGS300, OYSGS- (300 mg/kg) and OVA-exposed mice; OVA+OYSGS500, OYSGS- (500 mg/kg) and OVA-exposed mice. Results are presented as means  $\pm$  SD (##  $p < 0.01$  compared with the NC group; \*  $p < 0.05$ , \*\*  $p < 0.01$  compared with the OVA group).

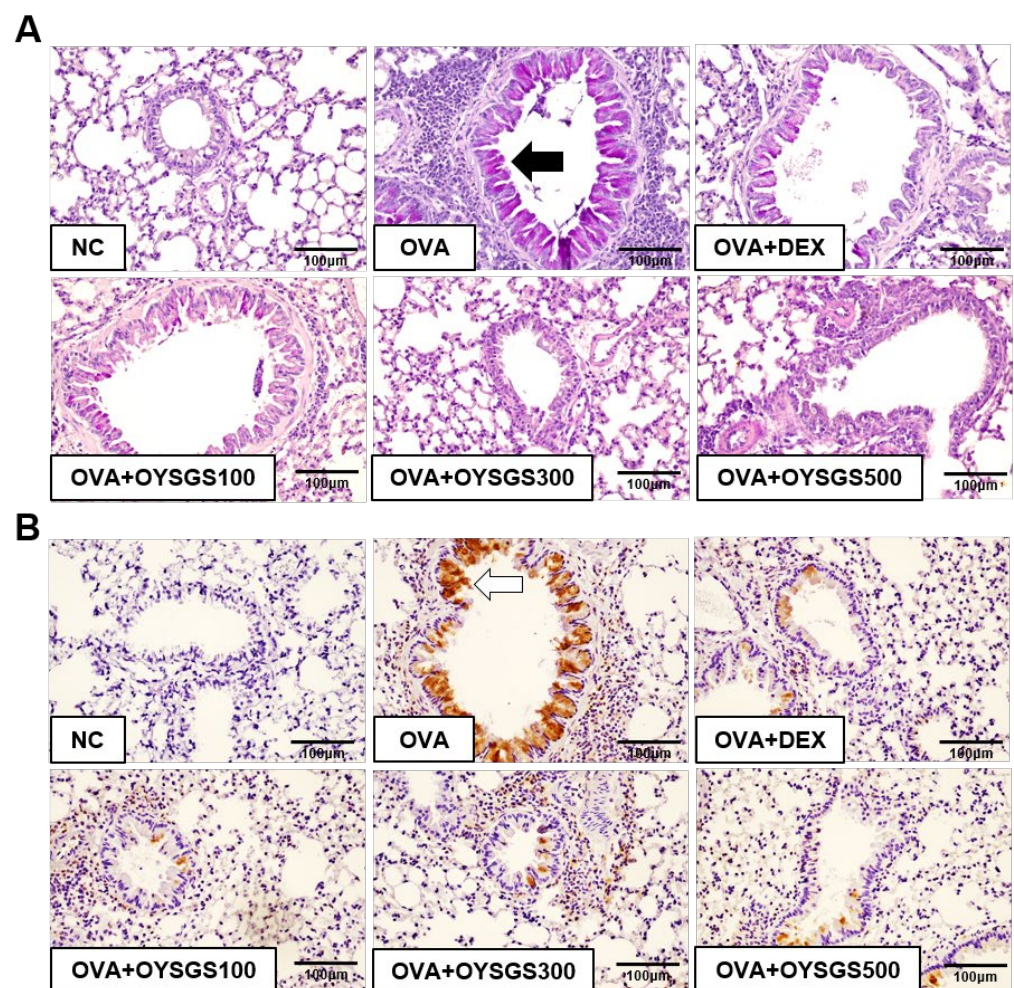


**Figure 5.** Cont.



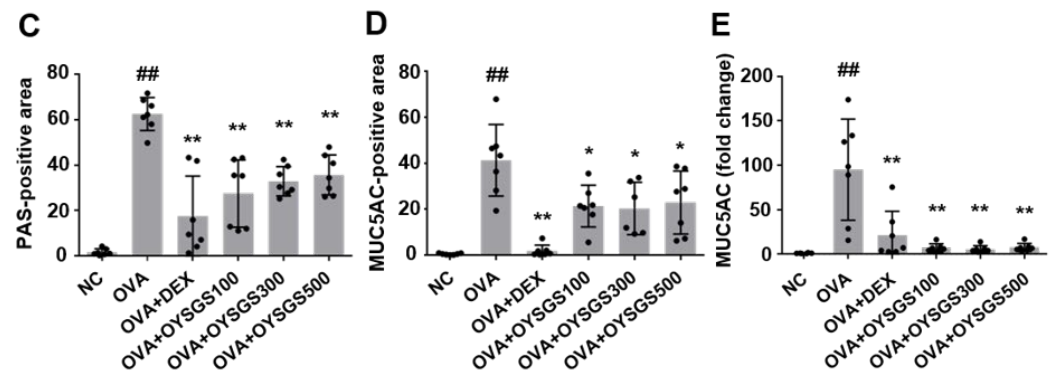


**Figure 5.** Effect of OYSGS on airway mucus production and goblet cell hyperplasia. (A) Representative images of PAS staining in lung tissues. Black arrow indicates the PAS-positive area significantly increased in the OVA tissue. Scale bar, 100  $\mu$ m; magnification, 200 $\times$  (B) Representative images showing immunohistochemistry of MUC5AC in lung tissues. White arrow indicates the MUC5AC-positive area significantly increased in the OVA tissue. Scale bar, 100  $\mu$ m; magnification, 200X. (C,D) PAS-positive area (C) and MUC5AC-positive area (D) were calculated based on the total area of the airway epithelium. (E) MUC5AC expression levels assessed by real-time RT-PCR. NC, negative control; OVA, ovalbumin-exposed mice; OVA+DEX, dexamethasone-administered and OVA-exposed mice; OVA+OYSGS100, OYSGS- (100 mg/kg) and OVA-exposed mice; OVA+OYSGS300, OYSGS- (300 mg/kg) and OVA-exposed mice; OVA+OYSGS500, OYSGS- (500 mg/kg) and OVA exposed mice. Results are presented as means  $\pm$  SD (<sup>##</sup>  $p < 0.01$  compared with the NC group; \*  $p < 0.05$ , <sup>\*\*</sup>  $p < 0.01$  compared with the OVA group).

### 3.6. Analysis of Oxidative Stress in Lung Tissues

A significant decrease in MDA concentration was observed in the OVA+OYSGS group compared to the OVA group (Figure 6A). Total glutathione was considerably higher in the OVA+DEX and OVA+OYSGS groups compared to the OVA group (Figure 6B). The changes did not differ across the tested concentrations of OYSGS, but they do indicate that OYSGS treatment reduces oxidative stress in lung tissues.

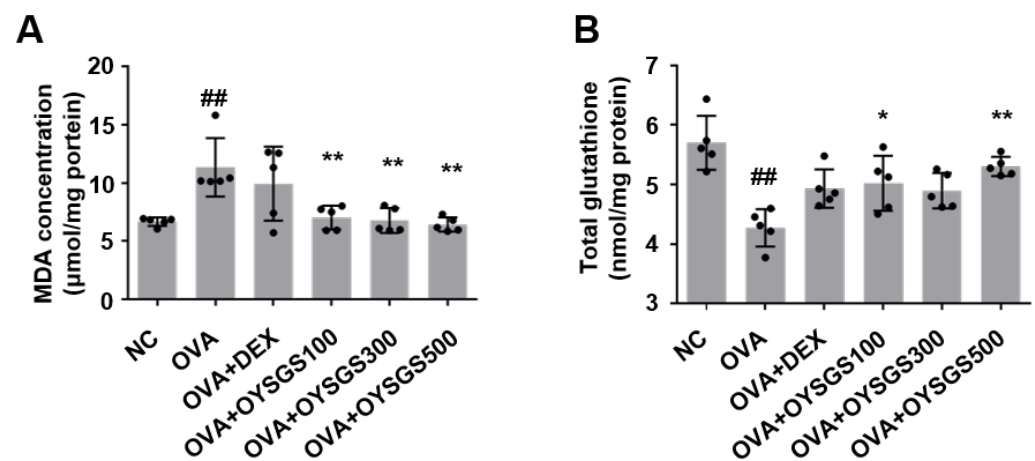


**Figure 6.** Effect of OYSGS on oxidative stress. (A,B) MDA (A) and total glutathione (GSSG/GSH) (B) levels in lung tissues, as assessed using ELISA. NC, negative control; OVA, ovalbumin-exposed mice; OVA+DEX, dexamethasone-administered and OVA-exposed mice; OVA+OYSGS100, OYSGS- (100 mg/kg) and OVA-exposed mice; OVA+OYSGS300, OYSGS- (300 mg/kg) and OVA-exposed mice; OVA+OYSGS500, OYSGS- (500 mg/kg) and OVA-exposed mice. Results are presented as means  $\pm$  SD (<sup>##</sup>  $p < 0.01$  compared with the NC group; \*  $p < 0.05$ , <sup>\*\*</sup>  $p < 0.01$  compared with the OVA group).

### 3.7. Analysis of p38 MAPK Expression

To begin elucidating the molecular action mechanism of OYSGS, we explored its potential effects on the p38 MAPK pathway. This investigation was prompted by reports indicating that p38 MAPK phosphorylation plays a critical role in triggering inflammatory responses in the lungs [43–45]. Western blot analysis revealed that phosphorylated p38 MAPK was notably decreased in the OVA+DEX and OVA+OYSGS groups compared to the OVA group (Figure 7).

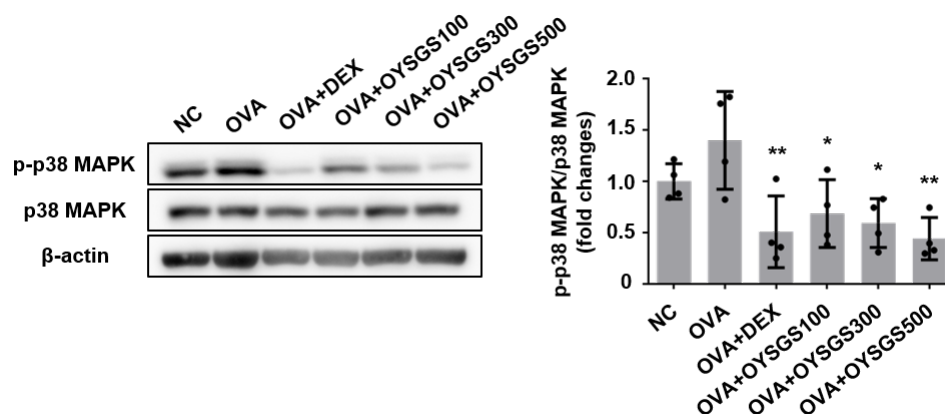


**Figure 7.** Effect of OYSGS on p38 MAPK activity in lung tissues. Phospho-p38 MAPK, p38 MAPK, and  $\beta$ -actin expression in lung tissues, as assessed by Western blotting. NC, negative control; OVA, ovalbumin-exposed mice; OVA+DEX, dexamethasone-administered and OVA-exposed mice; OVA+OYSGS100, OYSGS- (100 mg/kg) and OVA-exposed mice; OVA+OYSGS300, OYSGS- (300 mg/kg) and OVA-exposed mice; OVA+OYSGS500, OYSGS- (500 mg/kg) and OVA-exposed mice. Results are presented as means  $\pm$  SD (\*  $p < 0.05$ , \*\*  $p < 0.01$  compared with the OVA group).

## 4. Discussion

In this study, we investigated the potential ability of OYSGS to inhibit asthma symptoms in an OVA-induced mouse model. In OVA-exposed mice, OYSGS was found to inhibit inflammatory cell recruitment and cytokine levels in BALF and lung tissues, reduce mucus production and oxidative stress, and attenuate p38 MAPK phosphorylation.

Asthma is a chronic respiratory condition typified by enduring inflammation of the airways. It arises from a multifaceted interplay of diverse factors that act upon intricate pathogenic mechanisms. When administered in the respiratory system, ovalbumin acts as a specific allergen to provoke immune responses, including T-cell sensitization [46,47]. Upon activation, T cells initiate a Th2 cell response that is characterized by phosphorylation of p38 MAPK, which, in turn, prompts the secretion of diverse pro-inflammatory cytokines [43–45,48]. Key Th2 cell-secreted cytokines, such as IL-5 and IL-13, contribute to the induction of airway inflammation [27,49]. Activated p38 MAPK may also recruit neutrophils and lymphocytes [50,51]. At sites of inflammation, neutrophils rapidly infiltrate and function as significant modulators of both inflammation and immune responses [52]. Lymphocytes, including T cells and B cells, contribute to adaptive immunity [53]. Their recruitment regulates the production of cytokines and chemokines to intensify inflammation [54]. In the current study, OYSGS treatment of OVA-induced mice was found to notably diminish inflammatory cell infiltration into lung tissues, decrease inflammatory cell counts in BALF, and reduce pro-inflammatory cytokine levels in BALF. It can be inferred from these observations that OYSGS inhibits the inflammatory response associated with asthma.

The asthma-related inflammatory response also leads to excessive mucus secretion. As mucus production increases, there are marked increases in the levels of glycoprotein in goblet cells and those of MUC5AC within the airway [55,56]. This heightened production of MUC5AC in the airways is a hallmark of asthma [3]. Increased mucus production exacerbates airflow obstruction in several ways. Initially, the surplus mucus physically constricts the airway passages, complicating the flow of air in the lungs. The increased

mucus also provides an ideal environment for the entrapment of airborne particles, such as allergens and pathogens, further contributing to worsened airway inflammation and bronchoconstriction [57]. Moreover, the chronic presence of mucus provides a breeding ground for bacterial colonization, which can lead to recurrent infections and perpetuation of the inflammatory response [58]. Here, we show that OYSGS treatment of OVA-induced mice significantly reduced the lung levels of both glycoprotein and MUC5AC expression, indicating that OYSGS inhibits asthma-related mucus production.

In the context of asthma, excess oxidative stress is intimately linked to reactive oxygen species (ROS) in the lungs. Th2-generated p38 MAPK recruits infiltrated neutrophils, which release ROS to enhance tissue damage [8]. The increased oxidative stress caused by neutrophils leads to re-escalation of p38 MAPK phosphorylation, thereby enhancing the destructive response characteristic of asthma [59]. ROS can impair the lungs' natural antioxidant defenses, which, in turn, disrupts the balance of redox processes [60]. More specifically, ROS can harm cellular components, such as by causing lipid peroxidation, protein oxidation, and DNA histone modification [61]. Inflammation further amplifies the production of ROS, which alters transcription factor profiles to initiate cellular stress responses [61]. Thus, it is crucial to effectively manage oxidative stress when seeking to improve asthma. In this report, we reveal that OYSGS treatment significantly attenuated oxidative stress in lung tissues, as shown by improvement in the levels of MDA and total glutathione.

Regarding potential underlying mechanisms of such effects, a previous study showed that OYSGS inhibits colon cancer cell proliferation by regulating the MAPK pathway [11]. Since the p38 MAPK pathway is known to play a significant role in asthma [43], we hypothesized that OYSGS might influence p38 MAPK. Indeed, we found that mice exposed to ovalbumin exhibited increased p38 MAPK phosphorylation, which has been linked to the elevation of inflammatory factors, such as IL-5 and IL-13, as well as recruitment of neutrophils and lymphocytes. We found that OYSGS appears to mitigate asthma-related inflammatory processes by inhibiting p38 MAPK phosphorylation to downregulate its downstream signaling pathways and thereby decrease pro-inflammatory cytokine levels and inflammatory cell recruitment. Downregulation of IL-5 and IL-13 also contributes to reducing mucus production, as evident from the differences observed in the lung tissue levels of glycoprotein and MUC5AC. OYSGS is also effective in attenuating oxidative stress, as indicated by improvements in the levels of MDA and total glutathione.

One limitation of this study is that we did not address the side effects of the substances comprising OYSGS. For instance, ephedrine, which makes up the second largest portion, has bronchodilator effects but also causes cardiovascular side effects [62,63]. Narirutin, the third largest component, has anti-inflammatory properties but is known to cause headaches and liver failure [64,65]. Therefore, further research is needed to understand the comprehensive impact of these side effects.

In summary, we have revealed that OYSGS has a protective effect against OVA-induced asthma in mice by reducing inflammation, oxidative stress, and mucus production. These improvements could be related to the inhibition of the p38 MAPK pathway. Although further research is needed to explore the side effects, these findings suggest that OYSGS can be considered a promising candidate for asthma treatment.

**Supplementary Materials:** The following supporting information can be downloaded at <https://www.mdpi.com/article/10.3390/app14125280/s1>, Table S1: Compounds identified in OYSGS by UPLC-DAD-MS/MS.

**Author Contributions:** Conceptualization, H.-J.K.; Methodology, E.-J.H., P.K., Y.-J.K. and M.-Y.L.; Formal Analysis, E.-B.B. and E.-J.H.; Investigation, J.-Y.S. and E.-B.B.; Writing and Original Draft, J.-Y.S. and H.-J.K.; Writing, Review, and Editing, H.-J.K. and E.-B.B.; Supervision, H.-J.K.; Project Administration, H.-J.K.; Funding Acquisition, H.-J.K. All authors have read and agreed to the published version of the manuscript.

**Funding:** This research was supported by grants from the Korea Institute of Oriental Medicine (grant number KSN1823221) and Chungnam National University.

**Institutional Review Board Statement:** The animal study protocol was approved by the Animal Experimental Ethics Committee of Chungnam National University, 2019012A-CNU-185.

**Informed Consent Statement:** Not applicable.

**Data Availability Statement:** The data that support the findings of this study are available from the corresponding author upon reasonable request.

**Conflicts of Interest:** The authors declare that they have no conflicts of interest.

## References

1. Lambrecht, B.N.; Hammad, H. The immunology of asthma. *Nat. Immunol.* **2015**, *16*, 45–56. [[CrossRef](#)] [[PubMed](#)]
2. Holgate, S.T. Innate and adaptive immune responses in asthma. *Nat. Med.* **2012**, *18*, 673–683. [[CrossRef](#)] [[PubMed](#)]
3. Evans, C.M.; Kim, K.; Tuvim, M.J.; Dickey, B.F. Mucus hypersecretion in asthma: Causes and effects. *Curr. Opin. Pulm. Med.* **2009**, *15*, 4. [[CrossRef](#)] [[PubMed](#)]
4. Rogers, D.F. Airway mucus hypersecretion in asthma: An undervalued pathology? *Curr. Opin. Pharmacol.* **2004**, *4*, 241–250. [[CrossRef](#)] [[PubMed](#)]
5. Sahiner, U.M.; Birben, E.; Erzurum, S.; Sackesen, C.; Kalayci, O. Oxidative stress in asthma. *World Allergy Organ. J.* **2011**, *4*, 151–158. [[CrossRef](#)] [[PubMed](#)]
6. Cho, Y.S.; Moon, H.-B. The role of oxidative stress in the pathogenesis of asthma. *Allergy Asthma Immunol. Res.* **2010**, *2*, 183–187. [[CrossRef](#)] [[PubMed](#)]
7. Papi, A.; Blasi, F.; Canonica, G.W.; Morandi, L.; Richeldi, L.; Rossi, A. Treatment strategies for asthma: Reshaping the concept of asthma management. *Allergy Asthma Clin. Immunol.* **2020**, *16*, 75. [[CrossRef](#)] [[PubMed](#)]
8. Mittal, M.; Siddiqui, M.R.; Tran, K.; Reddy, S.P.; Malik, A.B. Reactive oxygen species in inflammation and tissue injury. *Antioxid. Redox Signal.* **2014**, *20*, 1126–1167. [[CrossRef](#)] [[PubMed](#)]
9. Chung, K.F.; Wenzel, S.E.; Brozek, J.L.; Bush, A.; Castro, M.; Sterk, P.J.; Adcock, I.M.; Bateman, E.D.; Bel, E.H.; Bleecker, E.R.; et al. International ERS/ATS guidelines on definition, evaluation and treatment of severe asthma. *Eur. Respir. J.* **2014**, *43*, 343–373. [[CrossRef](#)]
10. Kim, Y.; So, H.-S.; Kim, J.-K.; Park, C.; Lee, J.-H.; Woo, W.-H.; Cho, K.-H.; Moon, B.-S.; Park, R. Anti-inflammatory effect of oyaksungisan in peripheral blood mononuclear cells from cerebral infarction patients. *Biol. Pharm. Bull.* **2007**, *30*, 1037–1041. [[CrossRef](#)]
11. Yim, N.-H.; Jung, Y.P.; Kim, A.; Ma, C.J.; Cho, W.K.; Ma, J.Y. Oyaksungisan, a traditional herbal formula, inhibits cell proliferation by induction of autophagy via JNK activation in human colon cancer cells. *Evid.-Based Complement. Altern. Med.* **2013**, *2013*, 231874. [[CrossRef](#)] [[PubMed](#)]
12. Kogure, T.; Sato, H.; Kishi, D.; Tatsumi, T. The effect of traditional herbal medicines; Uyakujunkisan on trigeminal neuralgia in an elderly patient—A case report and literature review. *Pain Pract.* **2008**, *8*, 408–411. [[CrossRef](#)] [[PubMed](#)]
13. Zhu, C.; Wang, M.; Guo, J.; Su, S.L.; Yu, G.; Yang, Y.; Zhou, Y.; Tang, Z. *Angelica dahurica* extracts attenuate CFA-induced inflammatory pain via TRPV1 in mice. *Evid.-Based Complement. Altern. Med.* **2022**, *2022*, 4684830. [[CrossRef](#)] [[PubMed](#)]
14. Luo, K.-W.; Sun, J.-G.; Chan, J.Y.-W.; Yang, L.; Wu, S.-H.; Fung, K.-P.; Liu, F.-Y. Anticancer effects of imperatorin isolated from *Angelica dahurica*: Induction of apoptosis in HepG2 cells through both death-receptor- and mitochondria-mediated pathways. *Chemotherapy* **2012**, *57*, 449–459. [[CrossRef](#)] [[PubMed](#)]
15. Hu, M.; Liu, Y.; He, L.; Yuan, X.; Peng, W.; Wu, C. Antiepileptic effects of protein-rich extract from *Bombyx batryticatus* on mice and its protective effects against H<sub>2</sub>O<sub>2</sub>-induced oxidative damage in PC12 cells via regulating PI3K/Akt signaling pathways. *Oxidative Med. Cell. Longev.* **2019**, *2019*, 7897584. [[CrossRef](#)] [[PubMed](#)]
16. Chen, S.-Y.; Zhou, Q.Y.-J.; Chen, L.; Liao, X.; Li, R.; Xie, T. The Aurantii Fructus Immaturus flavonoid extract alleviates inflammation and modulate gut microbiota in DSS-induced colitis mice. *Front. Nutr.* **2022**, *9*, 1013899. [[CrossRef](#)] [[PubMed](#)]
17. Nakamori, S.; Takahashi, J.; Hyuga, S.; Yang, J.; Takemoto, H.; Maruyama, T.; Oshima, N.; Uchiyama, N.; Amakura, Y.; Hyuga, M.; et al. Analgesic effects of Ephedra Herb extract, ephedrine alkaloids-free Ephedra Herb extract, ephedrine, and pseudoephedrine on formalin-induced pain. *Biol. Pharm. Bull.* **2019**, *42*, 1538–1544. [[CrossRef](#)]
18. Mashhadi, N.S.; Ghasvand, R.; Askari, G.; Hariri, M.; Darvishi, L.; Mofid, M.R. Anti-oxidative and anti-inflammatory effects of ginger in health and physical activity: Review of current evidence. *Int. J. Prev. Med.* **2013**, *4* (Suppl. 1), S36. [[PubMed](#)]
19. Kim, K.R.; Jeong, C.-K.; Park, K.-K.; Choi, J.-H.; Park, J.H.Y.; Lim, S.S.; Chung, W.-Y. Anti-inflammatory effects of licorice and roasted licorice extracts on TPA-induced acute inflammation and collagen-induced arthritis in mice. *J. Biomed. Biotechnol.* **2010**, *2010*, 709378. [[CrossRef](#)]
20. Park, E.-J.; Lee, H.-J. Immunomodulatory effects of fermented *Platycodon grandiflorum* extract through NF- $\kappa$ B signaling in RAW 264.7 cells. *Nutr. Res. Pract.* **2020**, *14*, 453–462. [[CrossRef](#)]

21. Xu, M.; Xu, Z.; Xu, Q.; Zhang, H.; Liu, M.; Geng, F.; Zhang, N. UPLC-MS/MS method for the determination of 14 compounds in rat plasma and its application in a pharmacokinetic study of orally administered Xiaoyao Powder. *Molecules* **2018**, *23*, 2514. [[CrossRef](#)] [[PubMed](#)]
22. Hwang, Y.-H.; Ma, J.Y. Preventive effects of an UPLC-DAD-MS/MS fingerprinted hydroalcoholic extract of *Citrus aurantium* in a mouse model of ulcerative colitis. *Planta Medica* **2018**, *84*, 1101–1109. [[CrossRef](#)] [[PubMed](#)]
23. Sont, J.K.; Han, J.; van Krieken, J.M.; Evertse, C.E.; Hooijer, R.; Willems, L.N.; Sterk, P.J. Relationship between the inflammatory infiltrate in bronchial biopsy specimens and clinical severity of asthma in patients treated with inhaled steroids. *Thorax* **1996**, *51*, 496–502. [[CrossRef](#)]
24. Wang, G.; Mohammadtursun, N.; Sun, J.; Lv, Y.; Jin, H.; Lin, J.; Kong, L.; Zhao, Z.; Zhang, H.; Dong, J. Establishment and evaluation of a rat model of sidestream cigarette smoke-induced chronic obstructive pulmonary disease. *Front. Physiol.* **2018**, *9*, 58. [[CrossRef](#)]
25. Kay, A. Asthma and inflammation. *J. Allergy Clin. Immunol.* **1991**, *87*, 893–910. [[CrossRef](#)] [[PubMed](#)]
26. Desai, D.; Brightling, C. Cytokines and cytokine-specific therapy in asthma. *Adv. Clin. Chem.* **2012**, *57*, 59.
27. Saha, S.K.; Berry, M.A.; Parker, D.; Siddiqui, S.; Morgan, A.; May, R.; Monk, P.; Bradding, P.; Wardlaw, A.J.; Pavord, I.D.; et al. Increased sputum and bronchial biopsy IL-13 expression in severe asthma. *J. Allergy Clin. Immunol.* **2008**, *121*, 685–691. [[CrossRef](#)]
28. Wadsworth, S.J.; Atsuta, R.; McIntyre, J.O.; Hackett, T.-L.; Singhera, G.K.; Dorscheid, D.R. IL-13 and TH2 cytokine exposure triggers matrix metalloproteinase 7-mediated Fas ligand cleavage from bronchial epithelial cells. *J. Allergy Clin. Immunol.* **2010**, *126*, 366–374.e8. [[CrossRef](#)]
29. Del Rio, D.; Stewart, A.J.; Pellegrini, N. A review of recent studies on malondialdehyde as toxic molecule and biological marker of oxidative stress. *Nutr. Metab. Cardiovasc. Dis.* **2005**, *15*, 316–328. [[CrossRef](#)]
30. Circu, M.L.; Aw, T.Y. Intestinal redox biology and oxidative stress. *Semin. Cell Dev. Biol.* **2012**, *23*, 729–737. [[CrossRef](#)]
31. Bonser, L.R.; Erle, D.J. Airway mucus and asthma: The role of MUC5AC and MUC5B. *J. Clin. Med.* **2017**, *6*, 112. [[CrossRef](#)] [[PubMed](#)]
32. Ma, J.; Rubin, B.K.; Voynow, J.A. Mucins, mucus, and goblet cells. *Chest* **2018**, *154*, 169–176. [[CrossRef](#)] [[PubMed](#)]
33. Rho, J.; Seo, C.-S.; Park, H.-S.; Jeong, H.-Y.; Moon, O.-S.; Seo, Y.-W.; Son, H.-Y.; Won, Y.-S.; Kwun, H.-J. Asteris Radix et Rhizoma suppresses testosterone-induced benign prostatic hyperplasia in rats by regulating apoptosis and inflammation. *J. Ethnopharmacol.* **2020**, *255*, 112779. [[CrossRef](#)] [[PubMed](#)]
34. Gao, Q.-H.; Wu, C.-S.; Wang, M. The jujube (*Ziziphus jujuba* Mill.) fruit: A review of current knowledge of fruit composition and health benefits. *J. Agric. Food Chem.* **2013**, *61*, 3351–3363. [[CrossRef](#)] [[PubMed](#)]
35. Lee, M.-K.; Kim, H.-W.; Kim, Y.J.; Lee, S.-H.; Jang, H.-H.; Jung, H.-A.; Kim, S.-B.; Lee, S.-H.; Choe, J.-S.; Kim, J.-B. Profiling of flavonoid glycosides in fruits and leaves of jujube (*Zizyphus jujuba* var. *inermis* (Bunge) Rehder) using UPLC-DAD-QTOF/MS. *Korean J. Food Preserv.* **2016**, *23*, 1004–1011. [[CrossRef](#)]
36. Zhou, J.-X.; Braun, M.S.; Wetterauer, P.; Wetterauer, B.; Wink, M. Antioxidant, cytotoxic, and Simultaneous Determination *Glycyrrhiza glabra* L., *Paeonia lactiflora* Pall., and *Eriobotrya japonica* (Thunb.) Lindl. extracts. *Medicines* **2019**, *6*, 43. [[CrossRef](#)]
37. Zhao, X.J.; Chen, D.; Kilmartin, P.A.; Jiao, B.N. Simultaneous determination of phenolics and polymethoxylated flavones in citrus fruits by ultra-high performance liquid chromatography coupled with triple-quadrupole mass spectrometry (UHPLC-QqQ-MS). *Anal. Lett.* **2019**, *52*, 1926–1938. [[CrossRef](#)]
38. Kim, H.G.; Kim, G.-S.; Lee, J.H.; Park, S.; Jeong, W.Y.; Kim, Y.-H.; Kim, J.H.; Kim, S.T.; Cho, Y.A.; Lee, W.S.; et al. Determination of the change of flavonoid components as the defence materials of Citrus unshiu Marc. fruit peel against *Penicillium digitatum* by liquid chromatography coupled with tandem mass spectrometry. *Food Chem.* **2011**, *128*, 49–54. [[CrossRef](#)]
39. Niu, C.; Sun, J.; Zheng, Y.; Wang, L.; Zhang, J.; Chen, R.; Ye, W. Determination of isosinensetin in rat plasma by UHPLC-MS/MS: Application to oral and intravenous pharmacokinetic study in healthy rats. *J. Pharm. Biomed. Anal.* **2020**, *184*, 113210. [[CrossRef](#)]
40. Zhang, J.; Zhang, Y.; Wang, Y. Validated quantification method for five ephedrine in dietary supplements using LC-MS/MS: Application to 503 cases. *J. Chromatogr. B* **2016**, *1039*, 1–7. [[CrossRef](#)]
41. He, Y.; Cheng, P.; Wang, W.; Yan, S.; Tang, Q.; Liu, D.; Xie, H. Rapid investigation and screening of bioactive components in simo decoction via LC-Q-TOF-MS and UF-HPLC-MD methods. *Molecules* **2018**, *23*, 1792. [[CrossRef](#)] [[PubMed](#)]
42. Zhang, H.; Gong, C.; Lv, L.; Xu, Y.; Zhao, L.; Zhu, Z.; Chai, Y.; Zhang, G. Rapid separation and identification of furocoumarins in *Angelica dahurica* by high-performance liquid chromatography with diode-array detection, time-of-flight mass spectrometry and quadrupole ion trap mass spectrometry. *Rapid Commun. Mass Spectrom.* **2009**, *23*, 2167–2175. [[CrossRef](#)] [[PubMed](#)]
43. Chung, K.F. p38 mitogen-activated protein kinase pathways in asthma and COPD. *Chest* **2011**, *139*, 1470–1479. [[CrossRef](#)] [[PubMed](#)]
44. Pelaia, C.; Vatrella, A.; Gallelli, L.; Lombardo, N.; Sciacqua, A.; Savino, R.; Pelaia, G. Role of p38 mitogen-activated protein kinase in asthma and COPD: Pathogenic aspects and potential targeted therapies. *Drug Des. Dev. Ther.* **2021**, *15*, 1275–1284. [[CrossRef](#)] [[PubMed](#)]
45. Newton, R.; Holden, N. Inhibitors of p38 mitogen-activated protein kinase: Potential as anti-inflammatory agents in asthma? *BioDrugs* **2003**, *17*, 113–129. [[CrossRef](#)] [[PubMed](#)]
46. Corry, D.B.; Grünig, G.; Hadeiba, H.; Kurup, V.P.; Warnock, M.L.; Sheppard, D.; Rennick, D.M.; Locksley, R.M. Requirements for allergen-induced airway hyperreactivity in T and B cell-deficient mice. *Mol. Med.* **1998**, *4*, 344–355. [[CrossRef](#)] [[PubMed](#)]

47. Kumar, R.K.; Herbert, C.; Foster, P.S. The “classical” ovalbumin challenge model of asthma in mice. *Curr. Drug Targets* **2008**, *9*, 485–494. [[CrossRef](#)] [[PubMed](#)]
48. Liang, L.; Li, F.; Bao, A.; Zhang, M.; Chung, K.F.; Zhou, X. Activation of p38 mitogen-activated protein kinase in ovalbumin and ozone-induced mouse model of asthma. *Respirology* **2013**, *18*, 20–29. [[CrossRef](#)] [[PubMed](#)]
49. Pelaia, C.; Paoletti, G.; Puggioni, F.; Racca, F.; Pelaia, G.; Canonica, G.W.; Heffler, E. Interleukin-5 in the pathophysiology of severe asthma. *Front. Physiol.* **2019**, *10*, 1514. [[CrossRef](#)]
50. Kim, D.; Haynes, C.L. The role of p38 MAPK in neutrophil functions: Single cell chemotaxis and surface marker expression. *Anal.* **2013**, *138*, 6826–6833. [[CrossRef](#)]
51. Risco, A.; Martin-Serrano, M.A.; Barber, D.F.; Cuenda, A. P38 $\gamma$  and P38 $\delta$  are involved in T lymphocyte development. *Front. Immunol.* **2018**, *9*, 65. [[CrossRef](#)] [[PubMed](#)]
52. Rosales, C. Neutrophil: A cell with many roles in inflammation or several cell types? *Front. Physiol.* **2018**, *9*, 113. [[CrossRef](#)]
53. Corrigan, C.; Hartnell, A.; Kay, A. T lymphocyte activation in acute severe asthma. *Lancet* **1988**, *331*, 1129–1132. [[CrossRef](#)]
54. Larché, M.; Robinson, D.S.; Kay, A. The role of T lymphocytes in the pathogenesis of asthma. *J. Allergy Clin. Immunol.* **2003**, *111*, 450–463. [[CrossRef](#)]
55. Kim, J.J.; Khan, W.I. Goblet cells and mucins: Role in innate defense in enteric infections. *Pathogens* **2013**, *2*, 55–70. [[CrossRef](#)] [[PubMed](#)]
56. Lachowicz-Scroggins, M.E.; Yuan, S.; Kerr, S.C.; Dunican, E.M.; Yu, M.; Carrington, S.D.; Fahy, J.V. Abnormalities in MUC5AC and MUC5B protein in airway mucus in asthma. *Am. J. Respir. Crit. Care Med.* **2016**, *194*, 1296–1299. [[CrossRef](#)] [[PubMed](#)]
57. Rutting, S.; Thamrin, C.; Cross, T.J.; King, G.G.; Tonga, K.O. Fixed airflow obstruction in asthma: A problem of the whole lung not of just the airways. *Front. Physiol.* **2022**, *13*, 898208. [[CrossRef](#)]
58. Siegel, S.J.; Weiser, J.N. Mechanisms of bacterial colonization of the respiratory tract. *Annu. Rev. Microbiol.* **2015**, *69*, 425–444. [[CrossRef](#)]
59. Han, X.; Hu, S.; Yang, Q.; Sang, X.; Tang, D.; Cao, G. Paeoniflorin ameliorates airway inflammation and immune response in ovalbumin induced asthmatic mice: From oxidative stress to autophagy. *Phytomedicine* **2021**, *96*, 153835. [[CrossRef](#)]
60. Rahman, I. Oxidative stress and gene transcription in asthma and chronic obstructive pulmonary disease: Antioxidant therapeutic targets. *Curr. Drug Targets-Inflamm. Allergy* **2002**, *1*, 291–315. [[CrossRef](#)]
61. Zuo, L.; Wijegunawardana, D. Redox role of ROS and inflammation in pulmonary diseases. In *Lung Inflammation in Health and Disease, Volume II*; Springer: Geneva, Switzerland, 2021; pp. 187–204.
62. Yoo, H.-J.; Yoon, H.-Y.; Yee, J.; Gwak, H.-S. Effects of ephedrine-containing products on weight loss and lipid profiles: A systematic review and meta-analysis of randomized controlled trials. *Pharmaceuticals* **2021**, *14*, 1198. [[CrossRef](#)] [[PubMed](#)]
63. May, C.; Pickup, M.; Paterson, J. The acute and chronic bronchodilator effects of ephedrine in asthmatic patients. *Br. J. Clin. Pharmacol.* **1975**, *2*, 533–537. [[CrossRef](#)] [[PubMed](#)]
64. Funaguchi, N.; Ohno, Y.; La, B.L.B.; Asai, T.; Yuhgetsu, H.; Sawada, M.; Takemura, G.; Minatoguchi, S.; Fujiwara, T.; Fujiwara, H. Narirutin inhibits airway inflammation in an allergic mouse model. *Clin. Exp. Pharmacol. Physiol.* **2007**, *34*, 766–770. [[CrossRef](#)] [[PubMed](#)]
65. Mitra, S.; Lami, M.S.; Uddin, T.M.; Das, R.; Islam, F.; Anjum, J.; Hossain, J.; Bin Emran, T. Prospective multifunctional roles and pharmacological potential of dietary flavonoid narirutin. *Biomed. Pharmacother.* **2022**, *150*, 112932. [[CrossRef](#)] [[PubMed](#)]

**Disclaimer/Publisher’s Note:** The statements, opinions and data contained in all publications are solely those of the individual author(s) and contributor(s) and not of MDPI and/or the editor(s). MDPI and/or the editor(s) disclaim responsibility for any injury to people or property resulting from any ideas, methods, instructions or products referred to in the content.